Experimental verification of a one-parameter scaling law for the quantum and "classical" resonances of the atom-optics kicked rotor

Sandro Wimberger,[1] Mark Sadgrove,[2] Scott Parkins,[2] and Rainer Leonhardt[2]
[1]*Dipartimento di Fisica E. Fermi, Università di Pisa, Largo Pontecorvo 3, 56127 Pisa, Italy*
[2]*Department of Physics, University of Auckland, Private Bag 92019, Auckland, New Zealand*
(Received 11 February 2005; published 12 May 2005)

We present experimental measurements of the mean energy in the vicinity of the first and second quantum resonances of the atom-optics kicked rotor for a number of different experimental parameters. Our data are rescaled and compared with the one-parameter (ϵ) classical scaling function developed to describe the quantum resonance peaks. Additionally, experimental data are presented for the "classical" resonance which occurs in the limit as the kicking period goes to zero. This resonance is found to be analogous to the quantum resonances, and a similar one-parameter classical scaling function is derived, and found to match our experimental results. The widths of the quantum and classical resonance peaks are compared, and their sub-Fourier nature examined.

DOI: 10.1103/PhysRevA.71.053404 PACS number(s): 42.50.Vk, 75.40.Gb, 05.45.Mt, 05.60.−k

I. INTRODUCTION

The heart of experimentally testing and controlling classical and quantum systems often lies in the introduction of an external periodic driving force [1–3]. The driving probes system-specific properties, the knowledge of which allows one, in turn, to understand and to optimally control the system at hand. In particular, driven systems often exhibit resonancelike behavior if the external driving frequency matches the natural frequency of the unperturbed system.

Typical nonlinear classical systems are resonant for only a finite interaction time since the driving itself forces the system to gain energy and hence drift out of resonance. Only if the natural frequencies are independent of the energy, as for the linear (harmonic) oscillator, the system can absorb energy on resonance indefinitely. In the quantum world, the situation may be different by virtue of the unperturbed system possibly having a discrete energy spectrum. If this spectrum shows an appropriate scaling in the excitation quantum number, resonant motion can persist forever.

A simple example of such a system is provided by the free rotor, whose energy spectrum scales quadratically in the excitation quantum number (due to periodic boundary conditions for the motion on the circle). Kicking the rotor periodically in time with a frequency commensurable with the energy difference of two neighboring levels leads to perfectly resonant driving. These so-called quantum resonances of the well-studied kicked rotor (KR) [4] have been known theoretically for some time [5], but the first traces of this example of frequency-matched driving have only recently come to light in experiments with cold atoms [6,7]. Such experiments [7] and theoretical studies [8,9] have also shown the surprisingly robust nature of these resonances in the presence of noise and perturbations.

Experimentally, the quantum resonances of the KR are hard to detect for two principal reasons. First, only a relatively small proportion of atoms are kicked resonantly for the following reason: ideally, the atomic motion is along a line, which introduces an additional parameter, namely, the noninteger part of the atomic momentum, i.e., the atom's quasimomentum. Treating the atoms independently, their motion can be mapped onto the circle owing to the spatial periodicity of the standing wave, which makes the quasimomentum a constant of the motion. However, only some values of quasimomentum allow resonant driving to occur [5]. All other values induce a dephasing in the evolution which hinders the resonant kicking of the atoms (see Sec. III for details). Second, if an atom is kicked resonantly it moves extremely quickly; in fact its energy grows quadratically in time (so-called ballistic propagation). These fast atoms quickly escape any fixed experimental detection window after a sufficiently large number of kicks [6,7].

In this paper, we report experimental data which show the behavior of a typical experimental ensemble of cold atoms under resonant driving. Our main observable is the mean energy of the atomic ensemble measured after a fixed number of kicks and scanned over the resonant kicking frequency or period. We verify a recently derived single-parameter scaling law of the resonant peak seen when scanning the energy vs the period [8,10,11]. The scaling law allows us to clearly resolve the resonance peak structure because it reduces the dynamics to a *stationary* and experimentally robust signature of the quantum resonant motion.

After a short review of our experimental setup in Sec. II and the theoretical treatment of the atom-optics kicked rotor close to quantum resonance in Sec. III, we present experimental data for the mean energies around the first two fundamental quantum resonances of the kicked atom. From these data, we extract the afore mentioned scaling law in Sec. IV. The effect of the quasimomentum (as a typical quantum variable) on the motion disappears in the classical limit of the kicked rotor, when the kicking period approaches zero [5,12]. In the latter case, the rotor is constantly driven, and a ballistic motion occurs for *all* members of the atomic ensemble [13]. Both phenomena, the quantum and the "classical" (for vanishing kicking period) resonance, are related to one another by a purely classical theory developed previously for the quantum resonance peaks [8,10,11].

In Sec. V we focus on the first direct comparison of the behavior of the ensemble averaged energies in the case of the "classical" and the quantum resonance. In particular, the sub-Fourier scaling of the resonance peaks in the mean energy as a function of the kick number is discussed. The latter makes both types of resonances studied here a potential source of high-precision measurements of system-specific parameters.

II. EXPERIMENTAL SETUP

Our experimental system is a realization of the paradigmatic kicked rotor model [14,15], whose relevance lies in the fact that it shows the basic features of a complex dynamical system, and it may be used to locally (in energy) approximate much more complicated systems, such as microwave-driven Rydberg atoms [16], or an ion in a particle accelerator [1,17].

Our experiments utilize a cloud of about 10^5 cold cesium atoms, provided by a standard six beam magneto-optical trap (MOT) [18]. The typical momentum spread of the atomic sample lies between four and eight two-photon recoils. The shape of the initial momentum distribution is well approximated by a Gaussian with standard deviation $\sigma_p \simeq (4-8) \times 2\hbar k_L$, centered at zero momentum [19], although significant non-Gaussian tails can exist [13]. The width is measured in units of two-photon recoils, corresponding to the wavelength of the kicking laser $\lambda_L = 2\pi/k_L$. The fractional parts in these units of the initial momenta, i.e., the quasimomentum discussed below, are practically uniformly distributed in the fundamental Brillouin zone defined by the periodic kick potential [10].

As shown in Fig. 1, the atoms interact with a pulsed, far-detuned optical standing wave which is created by retroreflecting the light from a 150 mW (slave) diode laser which is injection locked to a lower-power (master) diode laser at a wavelength of $\lambda_L = 852$ nm. Power fluctuations were minimal during the experiments performed here ($\sim 1\%$) although larger drifts occurred over the course of many experimental runs. Accurate pulse timing is achieved using a custom-built programmable pulse generator (PPG) to gate an acousto-optic modulator. The PPG is programmed by a computer running the RTLINUX™ operating system kernel [20] which controls the timing of the experimental sequence (aside from the pulse train itself). Experimentally, we approximate δ kicks by pulses of width τ_p which are approximately rectangular in shape. The lowest value of τ_p used in our experiments was 240 ns and the highest was 480 ns. For the experiments reported here, the effect of the finite width of the kicking pulses [19,22] turns out to be negligible, since fairly small numbers of kicks (fewer than 20) and low kicking strengths are used. In the case where the $\tau \to 0$ limit is being investigated experimentally, the δ-kick assumption is clearly not valid [13,21]. This restricts us to a minimum period $\tau = 320$ ns, for $\tau_p = 240$ ns, in our study of the "classical" resonance peaks.

In a typical experimental run, the cooled atoms were released from the MOT and subjected to up to 16 standing wave pulses, then allowed to expand for an additional free drift time in order to resolve the atomic momenta. After this expansion time, the trapping beam is switched on and the atoms are frozen in space by optical mollases. A charge-coupled device image of the resulting fluorescence is recorded and used to infer the momentum distribution of the atoms using standard time-of-flight techniques [6]. The mean energy of the atomic ensemble may then be inferred by calculating the second moment of the experimental momentum distribution.

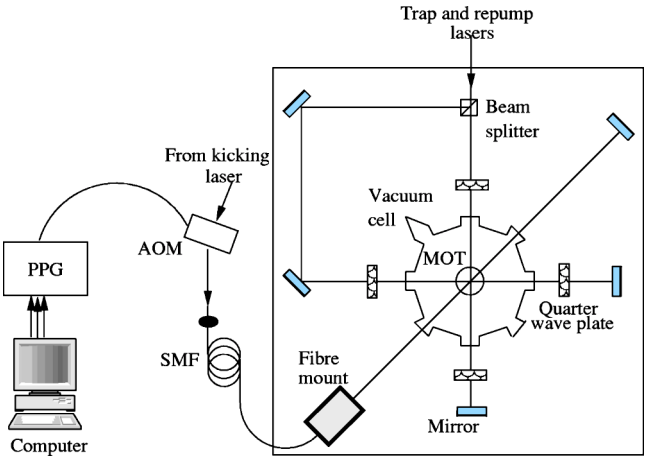

FIG. 1. Schematic diagram of our experimental setup. A standard six-beam magneto-optical trap (MOT) of about 10^5 Cs atoms is formed inside a vacuum cell at the intersection of three retroreflected "trapping" beams [vertical beams and (anti-)Helmholtz coils are not shown]. A standing wave is formed across the cloud of atoms by retroreflecting light from a "kicking laser," which is transported to the MOT by means of a single-mode fiber (SMF). This light is pulsed on and off by an acousto-optic modulator (AOM) which is gated by a programmable pulse generator (PPG). The PPG's pulse train is uploaded from a computer, which also controls the timing of the experiment (e.g., when the trapping AOM and anti-Helmholtz coils are turned on and off).

Kicking laser powers of up to 30 mW were employed, and detunings from the $6S_{1/2}(F=4) \to 6P_{3/2}(F'=5)$ transition of cesium of 500 MHz and 1 GHz were used for the classical and quantum resonance scans, respectively. These parameters produced spontaneous emission rates of $<0.5\%$ per kick for the quantum resonance scans, which was low enough to ensure that the structure of the peaks was not affected for the low kick numbers used here.

III. ϵ CLASSICAL DYNAMICS NEAR THE FUNDAMENTAL QUANTUM RESONANCES

We now consider the theoretical treatment of the atom-optics kicked rotor near quantum resonance. The Hamiltonian that generates the time evolution of the atomic wave function is (in dimensionless form) [6,14]

$$H(t') = \frac{p^2}{2} + k\cos(z)\sum_{t=0}^{N}\delta(t' - t\tau), \tag{1}$$

where p is the atomic momentum in units of $2\hbar k_L$ (i.e., of two-photon recoils), z is the atomic position in units of $2k_L$, t' is time, and t is an integer that counts the kicks. In our

units, the kicking period τ may also be viewed as a scaled Planck constant as defined by the equation $\tau=8E_RT/\hbar$, where $E_R=\hbar^2k_L^2/2M$ is the recoil energy (associated with the energy change of a cesium atom of mass M after emission of a photon of wavelength $\lambda_L=2\pi/k_L=852$ nm). The dimensionless parameter k is the kicking strength of the system and is proportional to the kicking laser intensity.

An atom periodically kicked in space and time is described by a wave packet $\psi(z)$ decomposed into 2π-periodic Bloch states $\psi_\beta(z)$, that is,

$$\psi(z)=\int_0^1 d\beta\,\exp(i\beta z)\psi_\beta(z), \tag{2}$$

where β is the quasimomentum (i.e., the fractional part of the momentum p). Quasimomentum is conserved in the evolution generated by Eq. (1), so the different Bloch states in Eq. (2) evolve independently of each other, whereby their momenta can change only by integers by virtue of the kicks. For any given quasimomentum, the dynamics is formally equivalent to that of a rotor (moving on a circle) whose one-period Floquet operator is given by

$$\hat{\mathcal{U}}_\beta=e^{-ik\cos(\hat{\theta})}e^{-i\tau(\hat{\mathcal{N}}+\beta)^2/2}, \tag{3}$$

where $\theta=z \bmod(2\pi)$, and $\hat{\mathcal{N}}=-id/d\theta$ is the angular momentum operator. From Eq. (3) we can immediately derive the two necessary conditions for quantum resonant motion: if $\tau=2\pi r/q$ $(r,q$ integers) then the atomic motion may show asymptotic quadratic growth in energy so long as $\beta=m/2r$, $0\leqslant m\leqslant 2r$, m integer at the same time. Under these conditions the Floquet operator (3) is also periodic in momentum space, with the integer period q. As in previous experimental studies [6], we focus on the first two fundamental quantum resonances $q=1$, 2, for which the amplitudes of Bloch waves with $\beta=1/2$ for $q=2$, and $\beta=0,1/2$ for $q=1$ at momentum states separated by $q\times 2\hbar k_L$ exactly rephase after each kick. The rephasing condition enforces ballistic propagation of the corresponding states in momentum space, so their energy grows quadratically in time. The remaining Bloch components of the original wave packet (2), with β not in the resonant class, exchange energy with the kicking laser in a quasiperiodic manner. The competition between the resonant and the nonresonant subclasses of Bloch states (between ballistic and quasiperiodic propagation) leads to *linear* growth of the total mean energy $E\approx k^2t/4$ obtained by incoherently averaging over the continuous set of quasimomenta which constitute the atomic ensemble [8,10,11].

For $q=1$, 2, we write $\tau=2\pi\ell+\epsilon$, where ϵ denotes the detuning from the exact resonance and $\ell=1$, 2. As shown in [10,11], the Floquet operator (3), can then be rewritten as

$$\hat{\mathcal{U}}_\beta(t)=e^{-i\tilde{k}\cos(\hat{\theta})/|\epsilon|}e^{-i\hat{\mathcal{H}}_\beta/|\epsilon|}, \tag{4}$$

with $\tilde{k}=k|\epsilon|$, $\hat{I}=|\epsilon|\hat{\mathcal{N}}$ as rescaled momentum, and

$$\hat{\mathcal{H}}_\beta(\hat{I},t)=\frac{1}{2}\mathrm{sgn}(\epsilon)\hat{I}^2+\hat{I}(\pi\ell+\tau\beta). \tag{5}$$

Introducing the new variables $J=\pm I+\pi\ell+\tau\beta$, $\vartheta=\theta+\pi[1-\mathrm{sgn}(\epsilon)]/2$, where $\pm$ denotes the sign of $\epsilon=\mathrm{sgn}(\epsilon)$, the quantum evolution can be approximated by the ϵ classical standard map derived in [10,11,23]:

$$J_{t+1}=J_t+\tilde{k}\sin(\vartheta_{t+1}),\quad \vartheta_{t+1}=\vartheta_t+J_t \tag{6}$$

for $\tilde{k}\ll 1$. J_t implicitly contains the quasimomentum β, which defines the initial conditions in momentum in the phase space generated by the map (6) [8].

For small $|\epsilon|$, the ϵ classical dynamics is quasi-integrable, and the growth of the energy is dominated by the principal ϵ classical resonant island around $J=2\pi$ [1]. The latter island is populated only by the values of β that are close to the resonant ones, while the nonresonant quasimomenta correspond to initial conditions outside the nonlinear resonance island [8,10,11]. Moreover, at any time t, the ratio between the energy and its value at $\epsilon=0$ is a scaling function of the *single* variable

$$x=t\sqrt{k|\epsilon|}. \tag{7}$$

The scaling function (which was explicitly derived in [8,10,11]) is

$$\frac{\langle E_{t,\epsilon}\rangle}{\langle E_{t,0}\rangle}\approx R(x)\equiv 1-\Psi_0(x)+\frac{4}{\pi x}G(x), \tag{8}$$

with the functions

$$\Phi_0(x)\equiv\frac{2}{\pi}\int_0^x ds\frac{\sin^2(s)}{s^2},$$

and

$$G(x)\approx\frac{1}{8\pi}\int_0^{2\pi}d\theta_0\int_{-2}^{2}dJ_0\overline{J}(x,\theta_0,J_0)^2.$$

$\overline{J}\equiv J/\sqrt{\tilde{k}}$ is the momentum of the pendulum approximation to the dynamics generated around the stable fixed point of (6), rescaled to unit coupling parameter (see [8,10,11] for details).

The one-parameter scaling law (8) allows us to deduce the shape and the parameter dependence of the resonance peaks elegantly from the experimental data, which in the unscaled form is shown in Figs. 2 and 3 for $\tau=2\pi$ and 4π, respectively.

IV. EXPERIMENTAL VERIFICATION OF THE SCALING LAW AT QUANTUM RESONANCE

We have used the data obtained for various scans of the mean energy vs the kicking period around the quantum resonances $\tau=2\pi$ and 4π, and for kick numbers $t=5$, 10, 15 to extract the ratio $\langle E_{t,\epsilon}\rangle/\langle E_{t,0}\rangle$. We subtract from the numerator the initial energy of the atomic ensemble with the characteristic width in momentum space σ_p. The contribution of $\sigma_p^2/2$ to the energy must be subtracted because the derivation of the scaling function $R(x)$ assumed an initial atomic momentum distribution in the unit interval $[0,1)$ [10], corresponding to a uniform distribution of quasimomenta $\beta\equiv p_0\in[0,1)$. Since the maximum of the resonance peak $\langle E_{t,\epsilon=0}\rangle$ is experimentally the most unstable parameter (due to the early loss

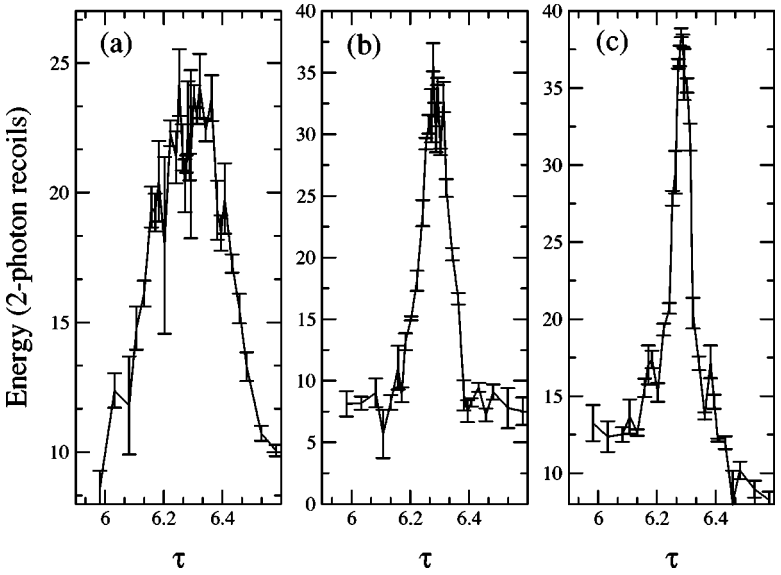

FIG. 2. Experimentally measured mean energies around the first quantum resonance at $\tau=2\pi$ after (a) 5, (b) 10, and (c) 15 kicks. Error bars show an average over three independent experiments. The kicking strength and initial momentum standard deviation were measured to be $k=4.1\pm0.6$ and $\sigma_p=5.9\pm0.2$, respectively. Note that the estimated errors in these parameters do not take into account systematic drifts which take place over the course of experimental runs. The solid line joins the experimental points to aid the eye.

of the fastest resonant atoms from the experimental detection window [6–8]), we use the theoretical value $\langle E_{t,0}\rangle-\sigma_p^2/2=k^2t/4$ to rescale our experimental data, rather than the height of the experimental peak itself. Results are presented in Figs. 4 and 5 for $\tau=2\pi$ and 4π respectively. We see very good agreement between the theoretical scaling function $R(x)$ from Eq. (8) and our experimental data. Despite the relatively large experimental errors due to the uncertainty in the determination of σ_p (see discussion below), the data show the characteristic structure, and also the oscillations arising from the contribution of the function $G(x)$ at large $x\geqslant 8$. These oscillations arise from the averaged contributions of the initial conditions $\overline{J_0}\in(-2,2)$ within the principal nonlinear resonance island, which evolve with different frequencies around the corresponding elliptic fixed point of the map (6). The quasimomentum classes contributing to $G(x)$ are thus the near-resonant values, while the nonresonant values contribute to the function $1-\Phi_0(x)$, which saturates to a constant for large x [8,10,11].

We fitted k and σ_p for each data set and then used these fitted parameters to scale our data. In the case of the $\tau=2\pi$ data, the best-fit value of k was found to be 4.5 compared to the independently measured value of $k=4.1\pm0.6$. For the $\tau=4\pi$ data, the best fit value of k was 5.2 compared with a measured value of $k=5\pm0.5$. The corresponding fitted values of σ_p were 5 and 5.2 two-photon recoils, respectively, which differ from the measured values of 4.53 ± 0.02 and 4.3 ± 0.2. This difference is due to the systematic error involved in determining σ_p from the experimental initial momentum distribution (as discussed in [13]). In particular this distribution may have noisy exponential wings [19] which must be truncated in order to reliably extract the second moment leading to an underestimation of the true initial momentum spread.

It is interesting to note that in Figs. 2 and 3, there is noticeable asymmetry in the resonance peaks. This degree of asymmetry is not predicted by the standard ϵ classical theory and its precise cause has not yet been ascertained. However, the asymmetry most likely stems from one or more systematic experimental effects, including the effect of small

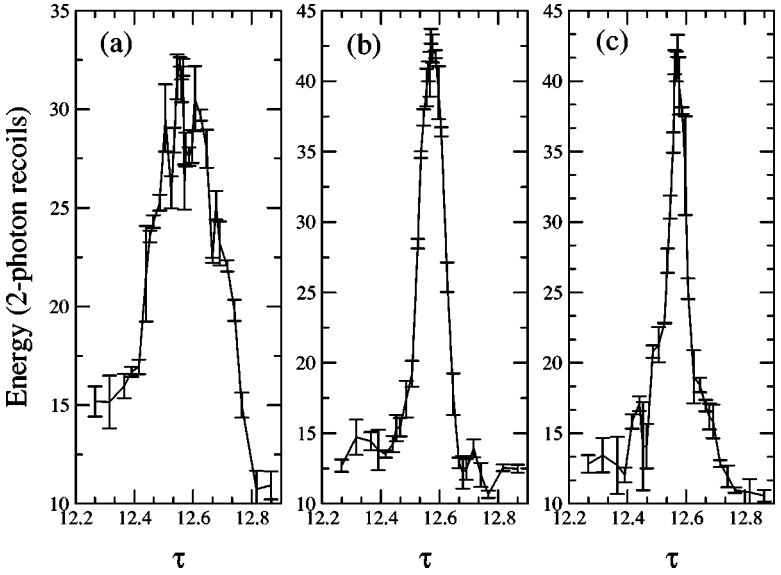

FIG. 3. Experimentally measured mean energies around the second quantum resonance at $\tau=4\pi$ for (a) 5; (b) 10, and (c) 15 kicks. The kicking strength and initial momentum standard deviation were measured to be $k=5.0\pm0.5$ and $\sigma_p=6.3\pm0.1$, respectively. Error bars as in Fig. 2. We note both in this figure and in Fig. 2 that the resonances exhibit some asymmetry, which is thought to be of purely experimental origin (see the discussion in Sec. IV).

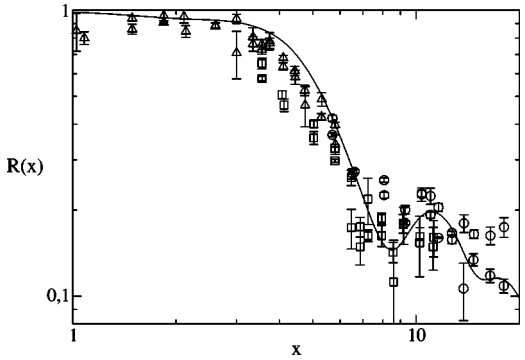

FIG. 4. Experimental mean energies around $\tau=2\pi$ taken from Fig. 2 and rescaled as $(\langle E_{t,\epsilon}\rangle-\sigma_p^2/2)/(tk^2/4)$. Triangles are for $t=5$, squares for $t=10$, and circles for $t=15$. Error bars represent statistical fluctuations over three experiments, and do not take into account fluctuations in k or σ_p. The solid line shows the numerically evaluated scaling function $R(x)$ of Eq. (8). We note that, for 10 and 15 kicks, data for $|\epsilon|<0.03$ have been omitted due to our inability to accurately resolve atomic energies for fast atoms this close to resonance. Experimental data for both positive and negative values of ϵ are plotted. We would like to note the good correspondence between the ϵ classical prediction and the experimental data for over one order of magnitude in the scaling variable x.

amounts of spontaneous emission ($<0.5\%$ chance per kick for the quantum resonance scans) and also from the slightly lesser time of flight experienced by atoms for positive as opposed to negative ϵ. Asymmetry of the peaks has also been noted in other experiments probing the structure of the quantum resonances [24]. In any case, this asymmetry does not prevent us from observing the structure of the quantum resonances, but leads to a slightly enhanced scatter of the experimental data points in Figs. 4 and 5.

V. CLASSICAL LIMIT OF VANISHING KICKING PERIOD

In spite of the intrinsically quantum nature of the quantum resonances as an example of perfectly frequency-matched driving, the method reviewed in Sec. III allows us to map the

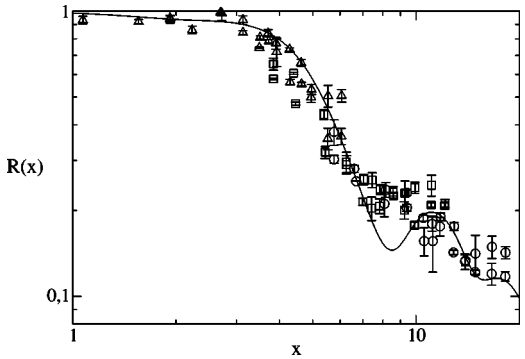

FIG. 5. Scaled experimental mean energies around $\tau=4\pi$ taken from Fig. 3; triangles are for $t=5$, squares for $t=10$, and circles for $t=15$ kicks. The solid line shows the scaling function $R(x)$ from Eq. (8). Again, for 10 and 15 kicks, data too close to resonance, i.e., for $|\epsilon|<0.03$, have been omitted.

quantum dynamics onto a purely classical map given by (6). The latter map is formally equivalent to the usual standard map, which describes the classical limit of the quantum KR when the kicking period tends to zero [12]:

$$J_{t+1}=J_t+\tilde{k}\sin(\theta_{t+1}),\quad \theta_{t+1}=\theta_t+J_t, \tag{9}$$

now with $J=\tau p=\tau(n+\beta)$ and $\tilde{k}=k\tau$. Because of the analogy between the maps (6) and (9), we expect a scaling law for the mean energy also in the limit $\tau\to 0$. Since $\tau\to 0$, all quasimomentum subclasses contribute now similarly to the energy growth, and the averaged energy is given only by the initial conditions within the principal nonlinear resonance island (see [13] for details)

$$\langle E_{t,\tau}\rangle \approx \tau^{-2}\langle (J_t)^2\rangle/2 \approx k/2\tau G_{\rm cl}(x), \tag{10}$$

with

$$G_{\rm cl}(x)\equiv \frac{\sqrt{k}}{2\pi\sqrt{\tau}}\int_0^{2\pi} d\theta_0 \int_0^{\sqrt{\tau k}} dJ_0 \overline{J}(x,\theta_0,J_0)^2$$

$$\approx \frac{1}{2\pi}\int_0^{2\pi} d\theta_0 \overline{J}(x,\theta_0,J_0=0)^2, \tag{11}$$

which depends on the variable $x=t(k\tau)^{1/2}$ [which, given that $\tau=\epsilon$ for the classical resonance, is the same as the scaling variable given in Eq. (7)] and weakly on k and τ, in *contrast* to the quantum resonant case studied in Sec. III. The dependence of $G_{\rm cl}$ on τ is negligibly small for $\tau\lesssim 1/k$, so that in practice $G_{\rm cl}$ can be viewed as a function of the scaling parameter x alone.

For the ratio $\langle E_{t,\tau}\rangle/\langle E_{t,0}\rangle$ we then arrive at the scaling function

$$\frac{\langle E_{t,\tau}\rangle}{\langle E_{t,0}\rangle}\approx R_{\rm cl}(x)\equiv \frac{2}{x^2}G_{\rm cl}(x), \tag{12}$$

which in the limit of vanishing τ tends to unity, since $G_{\rm cl}(x)\approx x^2/2$ for small x [8,13]. Our result (10) describes *quadratic* growth in mean energy as $\tau\to 0$. We note again that in the case of quantum resonances, ϵ classical theory predicts only *linear* mean energy growth with kick number at quantum resonance [10,11]. This linear increase is induced by the contribution of most quasimomentum classes which lie *outside* the classical resonance island. For $\tau\to 0$, almost all initial conditions (or quasimomenta) lie *within* the principal resonance island, which leads to the ballistic growth for the *averaged* ensemble energy (10).

For finite $\tau>0$ and $t^2k\gg 1/\tau$, we obtain from (10)

$$\langle E_{t,\tau>0}\rangle \approx \frac{k}{2\tau}\alpha, \tag{13}$$

since $G_{\rm cl}$ saturates to the value $\alpha\simeq 0.7$ for large x. Within the stated parameter range, this result implies dynamical freezing—the ensemble's mean energy is independent of kick number. This phenomenon is a classical effect in a system with a regular phase space, and was observed in [13] for the first time. It is distinct from dynamical localization which is the quantum suppression of momentum diffusion for a chaotic phase space [4,12]. Experimentally, the freezing ef-

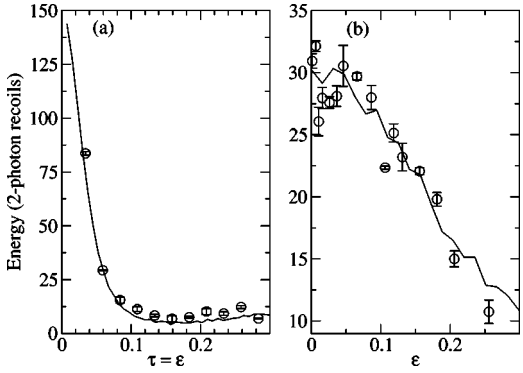

FIG. 6. (a) Circles show experimentally measured mean energies as $\tau \to 0$ after 5 kicks. The measured value of k is 4.9 ± 0.2. The solid line is classical data for $k=4.9$, as generated by the map (9), using practically the same initial momentum distribution as in the experiment. The thermal energy $\sigma_p^2/2$ has been subtracted to facilitate comparison with the quantum resonance curve in (b). In (b), circles show experimental data after 5 kicks near the second quantum resonance for positive $\epsilon = \tau - 4\pi$ and the experimental parameters are as given for Fig. 3. The thermal energy $\sigma_p^2/2$ has been subtracted. The solid line shows ϵ classical data as generated by the map (6).

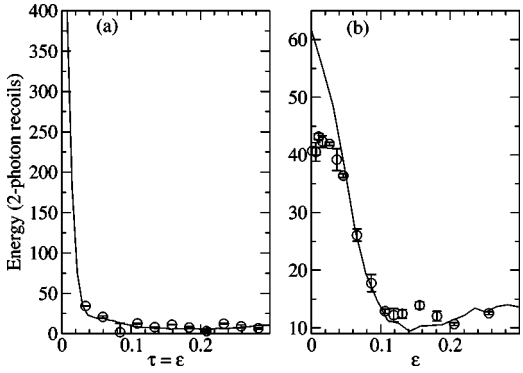

FIG. 7. (a) Circles show experimental data as $\tau \to 0$ for 10 kicks. The other experimental parameters are the same as those given for Fig. 6(a). The circles in (b) show experimental data once again for the second quantum resonance after 10 kicks this time. Other experimental parameters are the same as those given for Fig. 6(b). We note that for the quantum resonance in (b), the simulation and experimental results differ most markedly near the resonance peak. In this region ($\epsilon \lesssim 0.03$), some fast, resonant atoms are being lost from the experimental viewing area leading to a lower energy growth rate than predicted theoretically (see discussion in Secs. I and II). Note that in (a) it is not possible to probe low values of $\tau = \epsilon$ due to the finite width of the pulses.

fect corresponds to the cessation of energy absorption from the kicks, similar (but different in origin) to that which occurs at dynamical localization. The freezing may be explained as the averaging over all trajectories which start at momenta close to zero, and move with different frequencies about the principal elliptic fixed point of the map (9).

From Eq. (12), we immediately see that for the "classical" resonance $\tau \to 0$, the resonant peak width scales in time like $(kt^2)^{-1}$, as at the quantum resonances studied in Secs. III and IV. However, the tails of the classical resonance peak decay faster (proportionally to $1/x^2$) than those at quantum resonance [proportionally to $1/x$; cf. Eq. (8)]. This very fast shrinking of both types of resonance peaks is compared in Figs. 6 and 7.

Both types of these sensitive resonance peaks may serve as an experimental tool for determining or calibrating parameters in a very precise manner. Additionally, we note that the quadratic scaling in time at the quantum resonances and the "classical" resonance, respectively, is much faster and hence much more sensitive than the sub-Fourier resonances detected in a similar context by Szriftgizer and co-workers [25]. A detailed study of the quantum energy spectrum of the kicked atoms close to the two types of resonances is under way to clarify the origin of the observed sub-Fourier scaling of the resonance peaks.

Finally, we have plotted rescaled experimental data for the $\tau \to 0$ resonance against the scaling function of Eq. (12), as seen in Fig. 8. The scaling was performed using the fitted parameters as given in Figs. 6 and 7. We note that it is more difficult to extract the scaling from experimental data in the classical case, as opposed to the quantum case, because the peak of the extremely narrow resonance is difficult to probe. This leads to a larger uncertainty in the scaled energy and the points appear somewhat more scattered than those in Figs. 4 and 5. However, the points clearly agree much better with the classical scaling function from (12) than the ϵ classical scaling function (8) which is shown in Fig. 8 as a dash-dotted line. The clearly different scaling of the quantum and the "classical" resonant peaks goes along with the same rates at which the peaks become narrower with time in a sub-Fourier manner.

VI. CONCLUSIONS

In summary, we have experimentally confirmed a theoretically predicted one-parameter scaling law for the resonance peaks in the mean energy of a periodically kicked cold

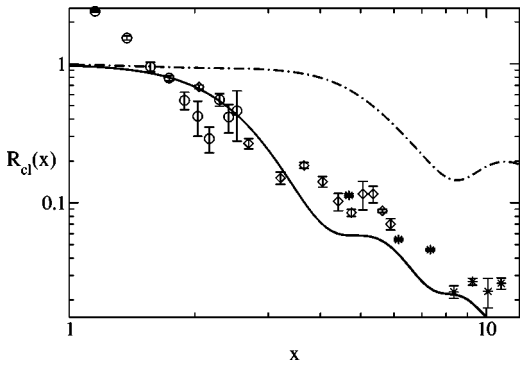

FIG. 8. Rescaled experimental mean energies for $\tau = 0.033 - 0.284$ (corresponding to $0.32 - 2.75$ μs). The data are for $k=4.9$ with $t=3$ (circles), 7 (diamonds), and 16 (stars). Error bars indicate statistical fluctuations over three experiments, and do not include variations in k or σ_p. The solid line shows the classical scaling function of Eq. (12). The dash-dotted line shows the scaling function from Eq. (8) (valid for the quantum resonances) for comparison.

atomic ensemble. This scaling of the resonant peaks is universal, in the sense that it reduces the dependence from all the system's parameters to just one combination of such variables. Furthermore, the scaling theory works in principle for arbitrary initial momentum distributions. In particular, it is valid for the experimentally relevant uniformly distributed quasimomenta at the fundamental quantum resonances of the kicked atoms. In the classical limit of vanishing kicking period, the dependence on quasimomentum, as an intrinsic quantum variable, disappears entirely, leading to a simpler version of the scaling law. The discussed scaling of the experimental data offers one the possibility to clearly observe the quantum and "classical" resonant peak structures over more than one order of magnitude in the scaling variable. Furthermore, its sensitive dependence on the system's parameters may be useful for high-precision calibration and measurements.

It will be of great interest to clarify whether a similar universal scaling law can be found for other time-dependent systems, such as the close-to-resonant dynamics of the kicked harmonic oscillator [26], or the driven Harper model [27,28]. As with the atom-optics kicked rotor, both of the latter systems may be readily realized in laboratory experiments [29,30].

ACKNOWLEDGMENTS

M.S. thanks T. Mullins for his assistance in the laboratory prior to these experiments and acknowledges support from the Tertiary Education Commission of New Zealand, Grant No. 03131. S.W. warmly thanks Professor Ennio Arimondo and Dr. Andreas Buchleitner for useful discussions and logistical support, and acknowledges funding by the Alexander von Humboldt Foundation and the Scuola di Dottorato di G. Galilei della Università di Pisa.

[1] A. L. Lichtenberg and M. A. Lieberman, *Regular and Chaotic Dynamics* (Springer, Berlin, 1992).
[2] J. E. Bayfield, *Quantum Evolution: An Introduction to Time-Dependent Quantum Mechanics* (Wiley, New York, 1999).
[3] W. Demtröder, *Laser Spectroscopy: Basic Concepts and Instrumentation* (Springer, Berlin, 2003).
[4] G. Casati *et al.*, in *Stochastic Behavior in Classical and Quantum Hamiltonian Systems*, edited by G. Casati and J. Ford (Springer, Berlin, 1979), p. 334.
[5] F. M. Izrailev and D. L. Shepelyansky, Sov. Phys. Dokl. **24**, 996 (1979); F. M. Izrailev, Phys. Rep. **196**, 299 (1999).
[6] W. H. Oskay *et al.*, Opt. Commun. **179**, 137 (2000); M. E. K. Williams *et al.*, J. Opt. B: Quantum Semiclassical Opt. **6**, 28 (2004); G. Duffy *et al.*, Phys. Rev. E **70**, 056206 (2004).
[7] M. B. d'Arcy *et al.*, Phys. Rev. Lett. **87**, 074102 (2001); Phys. Rev. E **69**, 027201 (2004); M. Sadgrove *et al.*, *ibid.* **70**, 036217 (2004).
[8] S. Wimberger, Ph.D. thesis, University of Munich and Università degli Studi dell' Insubria, 2004, available at http://edoc.ub.uni-muenchen.de/archive/00001687/
[9] S. Wimberger, R. Mannella, O. Morsch, and E. Arimondo, Phys. Rev. Lett. **94**, 130404 (2005); L. Rebuzzini, S. Wimberger, and R. Artuso, Phys. Rev. E **71**, 036220 (2005).
[10] S. Wimberger, I. Guarneri, and S. Fishman, Nonlinearity **16**, 1381 (2003).
[11] S. Wimberger, I. Guarneri, and S. Fishman, Phys. Rev. Lett. **92**, 084102 (2004).
[12] S. Fishman, in *Quantum Chaos*, Proceedings of the International School of Physics "Enrico Fermi", Course CXIX, edited by G. Casati *et al.* (IOS, Amsterdam, 1993).
[13] M. Sadgrove, S. Wimberger, S. Parkins, and R. Leonhardt, Phys. Rev. Lett. (to be published).
[14] R. Graham, M. Schlautmann, and P. Zoller, Phys. Rev. A **45**, R19 (1992).
[15] F. L. Moore *et al.*, Phys. Rev. Lett. **75**, 4598 (1995).
[16] G. Casati, I. Guarneri, and D. Shepelyansky, IEEE J. Quantum Electron. **24**, 1420 (1988); S. Wimberger and A. Buchleitner, J. Phys. A **34**, 7181 (2001).
[17] B. V. Chirikov, Phys. Rep. **52**, 263 (1979).
[18] C. Monroe, W. Swann, H. Robinson, and C. Wieman, Phys. Rev. Lett. **65**, 1571 (1990)
[19] B. G. Klappauf, W. H. Oskay, D. A. Steck, and M. G. Raizen, Physica D **131**, 78 (1999).
[20] FSMLabs Inc., http://www.fsmlabs.com/products/rtlinuxpro/rtlinuxpro_faq.html
[21] M. Sadgrove, T. Mullins, S. Parkins, and R. Leonhardt, Phys. Rev. E **71**, 027201 (2005).
[22] R. Blümel, S. Fishman, and U. Smilansky, J. Chem. Phys. **84**, 2604 (1986).
[23] S. Fishman, I. Guarneri, and L. Rebuzzini, J. Stat. Phys. **110**, 911 (2003); Phys. Rev. Lett. **89**, 084101 (2002).
[24] M. Hoogerland, S. Wayper, and W. Simpson (unpublished).
[25] P. Szriftgiser, J. Ringot, D. Delande, and J. C. Garreau, Phys. Rev. Lett. **89**, 224101 (2002); H. Lignier, J. C. Garreau, P. Szriftgiser, and D. Delande, Europhys. Lett. **69**, 327 (2005).
[26] G. M. Zaslavsky *et al.*, *Weak Chaos and Quasi-Regular Patterns* (Cambridge University Press, Cambridge, U.K., 1992); D. Shepelyansky and C. Sire, Europhys. Lett. **20**, 95 (1992); F. Borgonovi and L. Rebuzzini, Phys. Rev. E **52**, 2302 (1995); A. R. R. Carvalho and A. Buchleitner, Phys. Rev. Lett. **93**, 204101 (2004).
[27] P. Leboeuf, J. Kurchan, M. Feingold, and D. P. Arovas, Phys. Rev. Lett. **65**, 3076 (1990); T. Geisel, R. Ketzmerick, and G. Petschel, *ibid.* **66**, 1651 (1991); R. Artuso *et al.*, *ibid.* **69**, 3302 (1992); I. Guarneri and F. Borgonovi, J. Phys. A **26**, 119 (1993); I. Dana, Phys. Rev. E **52**, 466 (1995).
[28] O. Brodier, P. Schlagheck, and D. Ullmo, Phys. Rev. Lett. **87**, 064101 (2001); A. R. Kolovsky and H. J. Korsch, Phys. Rev. E **68**, 046202 (2003).
[29] H.-J. Stöckmann, *Quantum Chaos: An Introduction* (Cambridge University Press, Cambridge, U.K., 1999); T. M. Fromhold *et al.*, Nature (London) **428**, 726 (2004).
[30] S. A. Gardiner, J. I. Cirac, and P. Zoller, Phys. Rev. Lett. **79**, 4790 (1997); S. A. Gardiner *et al.*, Phys. Rev. A **62**, 023612 (2000).